Supporting Information

for

A Tetradentate Benzannulated P^N^N^P Ligand and Its Fe(II) Complex – Synthesis, Characterization, and Electrocatalytic Hydrogen Evolution

*Baldeep K. Sidhu, Amelia Kacperkiewicz, Jason D. Braun and David E. Herbert**

Department of Chemistry and the Manitoba Institute for Materials, University of Manitoba, 144 Dysart Road, Winnipeg, Manitoba, R3T 2N2, Canada; *david.herbert@umanitoba.ca

TABLE OF CONTENTS

EXPERIMENTAL DETAILS **3**
Materials **3**
Instrumentation and Methods **3**
SYNTHETIC PROCEDURES **4**
Determination of the Identity of Side Products Formed in the First Successful Attempt of Synthesizing L^L **4**
Figure S1. Crude $^{31}P\{^{1}H\}$ NMR spectrum ($CDCl_3$, 300 MHz, 22°C) of the quenched reaction mixture (top spectrum) showing assignments of **L** (-13.68 ppm), **L^L** (-14.99 ppm), **L-H₂** (-22.28 ppm) and [**L^L**]-**H₂** (-12.46 ppm and -22.69 ppm, blue and red circles), based on the spectrum of isolated **L-H₂** (middle spectrum) and **L** (bottom spectrum). 5
Optimization of Reaction Conditions for the Synthesis of P^N^N^P Ligand 4,4′-bis(diphenylphosphino)-2,2′-dimethyl-6,6′-biphenanthridine (L^L) **6**
Table S1. Optimization of reaction conditions for the synthesis of **L^L** 6
Preparation of 4,4′-Bis(diphenylphosphino)-2,2′-dimethyl-6,6′-biphenanthridine (L^L) **6**
Preparation of 1 ..... **7**
X-RAY CRYSTALLOGRAPHY **8**
Table S2. Crystal data and structure refinement parameters for compounds **L^L** and **1**. 10
UV-VIS ABSORPTION SPECTRA **11**
Figure S2. UV-vis absorption spectrum of **1** in acetonitrile. 11
Figure S3. UV-vis absorption spectrum of (a) **1** monitored over 64 h under constant white-light irradiation in an N_2 atmosphere. The gray traces correspond to spectra collected between 0 and 64 hours. (b) **1** monitored over 64 h when stored in the dark in an N_2 atmosphere. (c) Proligand **L^L**. (d) **1** monitored over 3 weeks when stored in the dark as a solution in aerated acetonitrile. 12
SUPPORTING INFORMATION FOR ELECTROCHEMICAL ANALYSIS **13**
Figure S4. The first reduction event of **1** in the absence and presence of trifluoroacetic acid (0, 4 and 8 mM, respectively) showing that this event remains reversible in the presence of excess acid. 13
Figure S5. Control experiments to show that there is no electrodeposition on the working electrode following electrocatalysis. The black trace represents a CV trace of 8 mM TFA in 0.1 M nBu$_4$PF$_6$ (i.e., the 'blank') showing the reduction of TFA at -1.7 V on glassy carbon electrode. The red trace shows the 50th cycle by CV of 1 mM **1** and 8 mM TFA indicating constant electrocatalysis. The blue trace represents a CV of a fresh solution of 8 mM TFA in 0.1 M nBu$_4$PF$_6$ using the same GC electrode replaced to this new solution following the CV cycling represented by the red trace. The blue trace shows the same current response as the initial blank, indicating no electrocatalysis. 14
Calculation of Overpotential (η) for HER Catalysis **14**
COMPUTATIONAL DETAILS **16**
Table S3. Comparison of experimental and calculated bond distances and angles obtained using O3LYP functional and different basis sets (geometry optimization done in the gas phase). ... 17
Table S4. Comparison of experimental and calculated bond distances and angles obtained using O3LYP functional and different basis sets (geometry optimization done in acetonitrile). 18

Table S5. Average percent error between experimental and calculated bond distances and angles. 19
NMR SPECTRA **20**
Figure S6. ^{1}H NMR spectrum ($CDCl_3$, 400 MHz, 22 °C) for **L^L**. 20
Figure S7. $^{31}P\{^{1}H\}$ NMR spectrum ($CDCl_3$, 121 MHz, 22 °C) for **L^L**. 21
Figure S8. $^{13}C\{^{1}H\}$ NMR spectrum ($CDCl_3$, 126 MHz, 22 °C) for **L^L**. 22
Figure S9. ^{1}H-^{1}H COSY NMR spectrum ($CDCl_3$, 500 MHz, 22 °C) of **L^L**. 23
Figure S10. ^{1}H-^{13}C HSQC NMR spectrum ($CDCl_3$, 500/125 MHz, 22 °C) of **L^L**. 24
Figure S11. ^{1}H-^{13}C HMBC NMR spectrum ($CDCl_3$, 500/125 MHz, 22 °C) of **L^L**. 25
Figure S12. ^{1}H NMR spectrum (CD_3CN, 300 MHz, 22 °C) for **1**. Asterisk indicates residual solvent (dichloromethane). 26
Figure S13. $^{13}C\{^{1}H\}$ NMR spectrum (CD_3CN, 126 MHz, 22 °C) for **1**. Asterisk indicates residual solvent (toluene). 27
Figure S14. $^{31}P\{^{1}H\}$ NMR spectrum (CD_3CN, 202 MHz, 22 °C) for **1**. 28
Figure S15. $^{19}F\{^{1}H\}$ NMR spectrum (CD_3CN, 471 MHz, 22 °C) for **1**. 29
HIGH RESOLUTION MASS SPECTRA **30**
Figure S16. HR-MS of **L^L** showing the $(M+H)^+$ ion. 30
Figure S17. HR-MS of **1** showing the M^+ ion of M = $(C_{52}H_{38}FeN_2P_2)(CF_3SO_3)$ which corresponds to the loss of the two acetonitrile units and one triflate counterion during ionization. 31
References 32

EXPERIMENTAL DETAILS

Materials

Unless otherwise specified, air-sensitive manipulations were carried either in a N_2 filled glove box or using standard Schlenk techniques under Argon. *N*-Iodosuccinimide (Combi Blocks), 2-Bromo-4-methylaniline (Combi Blocks), Trifluoroacetic acid (Sigma Aldrich), 2-Formylphenylboronic acid (Combi Blocks), $Pd(PPh_3)_4$ (Sigma Aldrich), Potassium carbonate (Fisher Scientific), *sec*-Butyllithium solution in hexanes (Sigma Aldrich), Chlorodiphenylphosphine (Sigma Aldrich), and Iron(II) trifluoromethanesulfonate (Sigma Aldrich) were purchased and used without further purification. Organic solvents (ACS grade) were dried and distilled using appropriate drying agents prior to use. Precursors 4-bromo-2-methylphenanthridine[1] and 4-diphenylphosphino-2-methylphenanthridine[2] were synthesized following published procedures.

Instrumentation and Methods

1- and 2D NMR spectra were recorded on Bruker Avance 300 MHz, Bruker Avance Neo 400 MHz, or Bruker Avance – III 500 MHz spectrometers. ^1H and $^{13}C\{^1H\}$ NMR spectra were referenced to residual solvent peaks.[3] High resolution mass spectra (HRMS) were recorded using a Bruker microOTOF-QIII. UV-vis absorption spectra were collected on a Cary 5000 UV-Vis-NIR spectrophotometer using 10 mm x 10 mm cuvettes (1 cm path length). For electrochemical analysis, 5-10 mg of the compound investigated was dissolved in 15 mL of 0.1 M (nBu$_4$N)PF_6 in CH_3CN. All electrochemical experiments were conducted under inert (Ar or N_2) atmosphere using a CHI 760c bipotentiostat, a 3 mm diameter glassy carbon working electrode, a Ag/Ag^+ non-aqueous quasi-reference electrode separated by a Vycor tip, and a Pt wire counter electrode. Cyclic voltammograms were collected at scan rates of 100-500 mV s^{-1} and differential pulse voltammograms were collected using a 5 mV increment, 50 mV amplitude, 0.1 s pulse width,

0.0167 s sample width, and 0.5 s pulse period. Upon completion of all CV and DPV analyses, ferrocene (FcH) was added to the solution as an internal standard, with all potentials reported versus the $FcH^{0/+}$ redox couple. Spectroelectrochemical experiments were performed using an air-tight room temperature OTTLE cell from the University of Reading. A three-electrode system of platinum working, auxiliary and Ag wire pseudo-reference electrodes was used.

SYNTHETIC PROCEDURES

Determination of the Identity of Side Products Formed in the First Successful Attempt of Synthesizing L^L

$^{31}P\{^{1}H\}$ NMR of the crude mixture in $CDCl_3$ showed peaks corresponding to five ^{31}P resonances with δ = -12.46 ppm, -13.68 ppm, -14.99 ppm, -22.28 ppm, and -22.69 ppm. This spectrum and the assignment of all side products observed in the spectrum is shown in Figure S1. The signal at -13.68 ppm corresponds to unreacted **L**. The peak at -22.28 ppm corresponds to 5,6-dihydro (2-methyl-4-diphenylphosphino) phenanthridine (**L-H₂**), as this chemical shift is consistent with the $^{31}P\{^{1}H\}$ chemical shift of **L-H₂** synthesized via chemical hydrogenation of **L** using $LiAlH_4$. The peaks at -12.46 ppm and -22.69 ppm are proposed to correspond to 5,6-dihydro-*bis*((2-methyl-4-diphenylphosphino) phenanthridyl) **[L^L]-H₂**, because the two P nuclei in **[L^L]-H₂** would be in non-equivalent chemical environments, and one of them is expected to have a chemical shift close to the chemical shift of the ^{31}P nucleus in **L**, while the other is expected to have a chemical shift close to the ^{31}P centre in **L-H₂**. The integrals of these two peaks are equal, which is expected for **[L^L]-H₂**. No peaks corresponding to the expected product 5,5',6,6'-tetrahydro-6,6'-*bis*((2-methyl-4-diphenylphosphino)phenanthridyl) **[L^L]-2H₂** were observed. After all other peaks in the crude NMR spectrum were assigned, the only signal left at δ = -14.99 ppm was proposed to correspond to the *P^N^N^P* dimer (**L^L**), because the chemical environment of ^{31}P in **L^L** is not

expected to differ substantially from its chemical environment in **L**, therefore its chemical shift would be relatively close to -13.68 ppm.

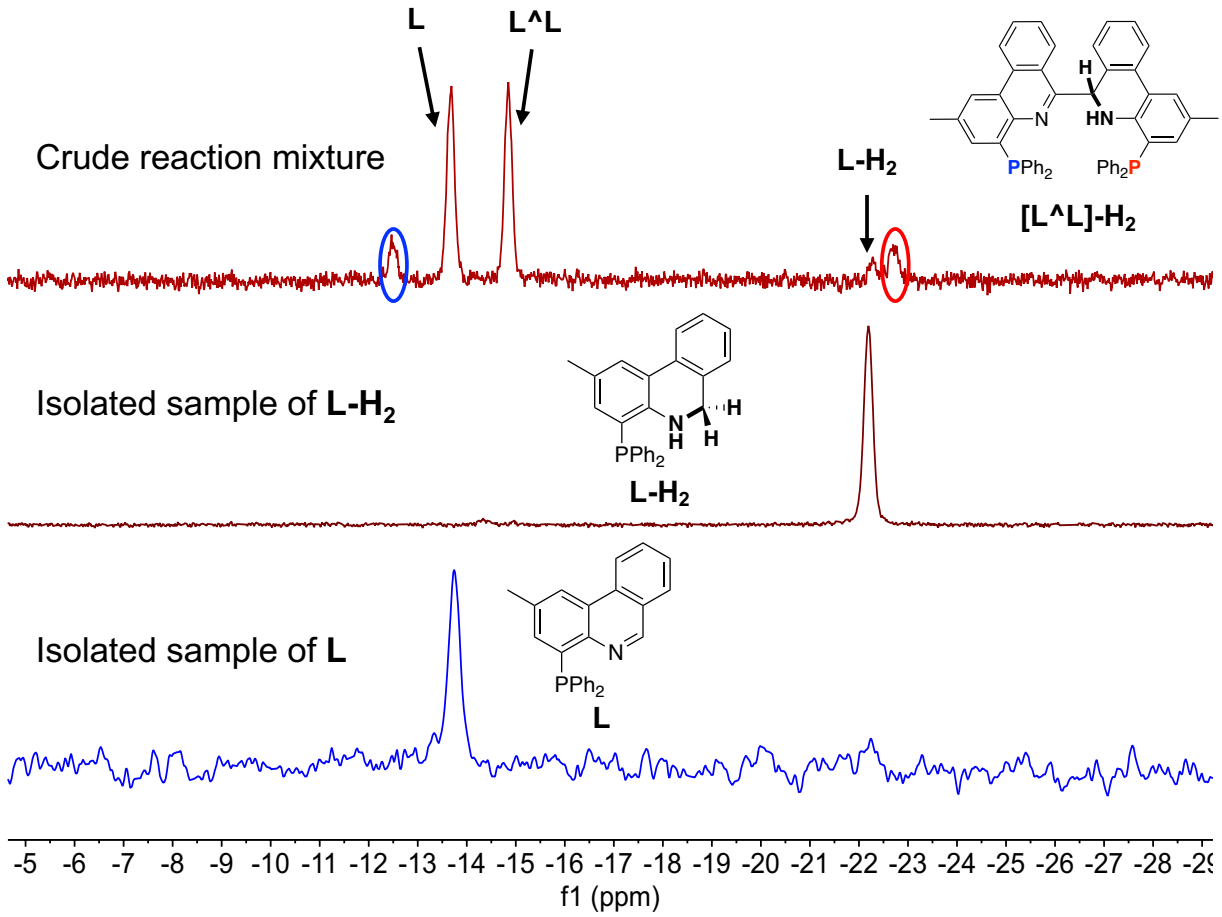

Figure S1. Crude $^{31}P\{^{1}H\}$ NMR spectrum ($CDCl_3$, 300 MHz, 22°C) of the quenched reaction mixture (top spectrum) showing assignments of **L** (-13.68 ppm), **L^L** (-14.99 ppm), **L-H$_2$** (-22.28 ppm) and **[L^L]-H$_2$** (-12.46 ppm and -22.69 ppm, blue and red circles), based on the spectrum of isolated **L-H$_2$** (middle spectrum) and **L** (bottom spectrum).

Optimization of Reaction Conditions for the Synthesis of P^N^N^P Ligand 4,4′-bis(diphenylphosphino)-2,2′-dimethyl-6,6′-biphenanthridine (L^L)

Table S1. Optimization of reaction conditions for the synthesis of **L^L**

Trial	Reaction scale / mmol	Reductant	Reflux duration / h	Eq. of H_2O added	Ratio[a] of L:L^L:L-H_2:[L^L]-H_2
1	0.0796	10 Na in amalgam[b]	48	excess	1:1:0.08:0.2
2	0.0796	10 Na in amalgam[b]	3	excess	0:0.2:1:1
3	0.0796	10 Na	3	excess	0:0:2:1
4	0.0796	1 K	48	1	0.5:1:0.4:0
5	0.0796	1 Na	12	1	0.2:1:0.4:0
6	0.265	1 Na	12	slight excess	0.1:0.5:1:1
7	0.265	1 Na	72	slight excess	0.3:1:0.96:0.8
8[c]	0.796	2 Na	72	1	0.2:1:0:0
9	**0.796**	**2 Na**	**72**	**0**	**0.2:1:0:0**

[a]via signal intensities of $^{31}P\{^1H\}$ NMR spectrum according to peak assignments in Figure S1

[b]amalgam = 5% Na in Hg

[c]reaction mixture filtered through a glass microfibre filter before adding water

Preparation of 4,4′-Bis(diphenylphosphino)-2,2′-dimethyl-6,6′-biphenanthridine (L^L)

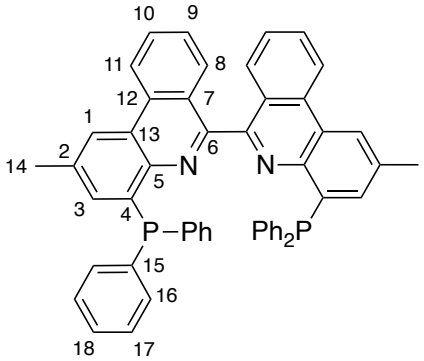

In a N_2-filled glovebox, a Teflon-stoppered flask was charged with 4-diphenylphosphino-2-methylphenanthridine (0.300 g, 0.796 mmol) and small pieces of sodium metal (0.037 g, 1.59 mmol), followed by toluene (18 mL). The flask was then sealed, taken out of the glovebox, and heated in an oil bath set to 110 °C for 4 d, during which the reaction mixture changed colour from yellow to olive green.

Upon cooling it down to room temperature, the mixture was filtered through a glass microfibre filter under a N_2 atmosphere, followed by passing additional toluene through the filter until colour stopped coming through. The solvent was then removed *in vacuo*, then the residue washed with minimal toluene (5 x 2 mL) to remove any unreacted starting material, and residual solvent removed under vacuum, leaving behind a light yellow solid. Isolated yield = 0.211 g (70%). ^{1}H NMR ($CDCl_3$, 400 MHz, 22 °C): δ 8.62 (d, $^3J_{HH}$ = 8.4 Hz, 1H, $C_{11}H$), 8.42 (s, 1H, C_1H), 7.64 (t, $^3J_{HH}$ = 7.7 Hz, 1H, $C_{10}H$), 7.50 (d, $^3J_{HH}$ = 8.3 Hz, 1H, C_8H), 7.37−7.32 (m, 2H, $^{Ph}C_{Ar}H$), 7.31−7.26 (m, 4H, $^{Ph}C_{Ar}H$), 7.22−7.17 (m, 4H, $^{Ph}C_{Ar}H$), 6.91 (dd, $^4J_{HH}$ = 3.8, 1.8 Hz, 1H, C_3H), 6.75 (t, $^3J_{HH}$ = 7.6 Hz, 1H, C_9H), 2.50 ppm (s, 3H, $C_{14}H_3$). ^{31}P{^{1}H} NMR ($CDCl_3$, 121 MHz, 22 °C): δ −14.99 ppm (s). ^{13}C{^{1}H} NMR ($CDCl_3$, 126 MHz, 22 °C): δ 155.85 (d, $^4J_{CP}$ = 2.3 Hz, C_6=N), 143.09 (d, $^2J_{CP}$ = 16.8 Hz, C_5), 138.92 (d, $^1J_{CP}$ = 11.8 Hz, C_4 or C_{15}), 138.80 (d, $^1J_{CP}$ = 12.3 Hz, C_4 or C_{15}), 137.24 (C_2), 135.08 (C_3), 134.38 (d, $^2J_{CP}$ = 20.4 Hz, C_{16}), 133.61 (d, $^{3/4}J_{CP}$ = 2.3 Hz, C_{12} or C_{13}), 129.87 (C_{10}), 128.98 (C_8), 128.44 (d, $^3J_{CP}$ = 6.9 Hz, C_{17}), 128.43 (C_{18}), 126.96 (C_9), 125.99 (C_7), 123.96 (d, $^{3/4}J_{CP}$ = 2.3 Hz, C_{12} or C_{13}), 122.63 (C_1), 121.77 (C_{11}), 22.40 ppm ($C_{14}H_3$). HR-MS (ESI-TOF/MS, m/z) calculated for M+H$^+$ (M = $C_{52}H_{38}N_2P_2$) 753.2583; found 753.2589.

Preparation of 1

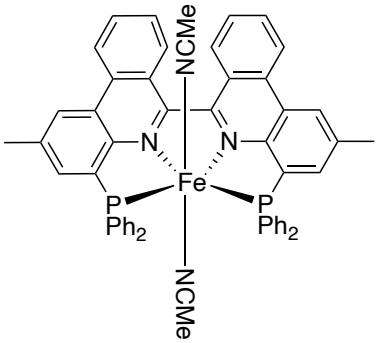

In a N_2-filled glovebox, **L^L** (0.050 g, 0.0665 mmol) was dissolved in CH_2Cl_2 (2mL) in a 20 mL scintillation vial. A solution of iron(II) trifluoromethanesulfonate (0.028 g, 0.0782 mmol) in acetonitrile (2 mL) was made separately and then added to the solution of **L^L**. The resulting suspension was allowed to stir at room temperature for 16 h in the dark, at which point a dark green solution had formed. This solution was filtered through a glass microfibre filter and solvent removed under reduced pressure,

leaving behind a dark green solid, which was pure by NMR. Isolated yield = 0.074 g (94 %). ^{1}H NMR (CD_3CN, 300 MHz, 22 °C): δ 9.12–9.10 (m, 2H, $^{Phen}C_{Ar}H$), 8.43 (d, $^{3}J_{HH}$ = 6.0 Hz, 1H, $^{Phen}C_{Ar}H$), 8.18–8.14 (m, 2H, $^{Phen}C_{Ar}H$), 7.79 (t, $^{3}J_{HH}$ = 7.5 Hz, 1H, $^{Phen}C_{Ar}H$), 7.55 (t, $^{3}J_{HH}$ = 7.5 Hz, 1H, $^{Ph}C_{Ar}H$), 7.48−7.44 (m, 1H, $^{Ph}C_{Ar}H$), 7.37-7.23 (m, 8H, $^{Ph}C_{Ar}H$), 2.81 ppm (s, 3H, CH_3). $^{31}P\{^{1}H\}$ NMR (CD_3CN, 202 MHz, 22 °C): δ 66.06 ppm (s). ^{19}F NMR (CD_3CN, 471 MHz, 22°C): δ -79.23 ppm (s). $^{13}C\{^{1}H\}$ NMR (CD_3CN, 126 MHz, 22 °C): δ 163.54 (C_{Ar}), 149.75 (C_{Ar}), 143.96 (C_{Ar}), 139.11 (C_{Ar}), 135.68 (C_{Ar}), 134.48 (C_{Ar}), 134.25 (C_{Ar}), 133.79 (C_{Ar}), 133.48 (C_{Ar}), 131.88 (d, J = 18.6 Hz, (C_{Ar}) , 130.29 (C_{Ar}), 130.07 (C_{Ar}), 128.68 (C_{Ar}), 128.14 (C_{Ar}), 127.71 (C_{Ar}), 127.04 (C_{Ar}), 124.66 (C_{Ar}), 22.46 ppm (CH_3). HR-MS (ESI-TOF/MS, m/z) calculated for M^+ [M = $(C_{52}H_{38}FeN_2P_2)(CF_3SO_3)$] 957.1374; found 957.1358.

X-RAY CRYSTALLOGRAPHY

Crystal structure parameters for L^L (CCDC 2487856): Crystals were grown by slow mixing of a layer of pentane with a solution in dichloromethane at -25 °C. Yellow blocks; $C_{52}H_{38}N_2P_2$ 752.78 g/mol, triclinic, space group P-1; a = 9.3919(6) Å, b = 14.2984(9) Å, c = 17.6937(11) Å, α = 80.538(2)°, β = 80.003(2), γ = 76.315(2)° V = 2254.6(2) Å^3; Z = 2, ρ_{calcd} = 1.109 g cm^{-3}; crystal dimensions 0.450 x 0.210 x 0.110 mm; $2\theta_{max}$ = 54.148°; 50409 reflections, 9831 independent (R_{int} = 0.0738), intrinsic phasing; absorption coeff (μ = 0.131 mm^{-1}), absorption correction semi-empirical from equivalents (SADABS); refinement (against F_o^2) with SHELXTL V6.1, 507 parameters, 0 restraints, R_1 = 0.0788 ($I > 2\sigma$) and wR_2 = 0.1803 (all data), Goof = 1.045, residual electron density 0.55/−0.49Å^{-3}. Residual solvent molecules could not be modelled successfully. A solvent void of 453 Å^3 containing an electron density of 123 e was dealt with using the SQUEEZE protocol included in the Olex 1.5 program. This is consistent with the presence of 1.5 molecules of pentane per formula unit.

Crystal structure parameters for 1 (CCDC 2487857): Crystals were grown by slow mixing of a layer of diethyl ether with a solution in acetonitrile at -25 °C. Green blocks; $C_{62}H_{50}N_2F_6FeN_6O_6P_2S_2$ 1261.92 g/mol, orthorhombic, space group $P2_12_12_1$; a = 12.553(4) Å, b = 17.050(5) Å, c = 27.154(10) Å, α = 90°, β = 90°, γ = 90° V = 5812(3) Å^3; Z = 4, ρ_{calcd} = 1.442 g cm^{-3}; crystal dimensions 0.325 x 0.117 x 0.066 mm; $2\theta_{max}$ = 49.526°; 65845 reflections, 9932 independent (R_{int} = 0.0755), intrinsic phasing; absorption coeff (μ = 0.463 mm^{-1}), absorption correction semi-empirical from equivalents (SADABS); refinement (against F_o^2) with SHELXTL V6.1, 507 parameters, 0 restraints, R_1 = 0.0820 ($I > 2\sigma$) and wR_2 = 0.2316 (all data), Goof = 1.091, Flack parameter = 0.30(4), residual electron density 0.94/−0.69Å^{-3}. Residual solvent molecules could not be modelled successfully. A solvent void of 384 Å^3 containing an electron density of 100 e was dealt with using the SQUEEZE protocol included in the Olex 1.5 program. This is consistent with the presence of 1 molecule of acetonitrile per formula unit.

Table S2. Crystal data and structure refinement parameters for compounds **L^L** and **1**.

Compound	**L^L**	**1**
Formula	$C_{52}H_{38}N_2P_2$	$C_{62}H_{50}N_2F_6FeN_6O_6P_2S_2$
Formula weight / g mol^{-1}	752.78	1261.92
Temperature / K	150	150
Crystal system	triclinic	orthorhombic
Space group	P-1	$P2_12_12_1$
a / Å	9.3919(6)	12.553(4)
b / Å	14.2984(9)	17.050(5)
c / Å	17.6937(11)	27.154(10)
α / º	80.538(2)	90
β / º	80.003(2)	90
γ / º	76.315(2)	90
Volume / Å^3	2254.6(2)	5812(3)
Z	2	4
ρ_{calcd} / g cm^{-3}	1.109	1.442
μ / mm^{-1}	0.131	0.463
F(000)	788.0	2580.0
Crystal dimensions / mm	0.450 x 0.210 x 0.110	0.325 × 0.117 × 0.066
Radiation	MoKα (λ = 0.71073)	MoKα (λ = 0.71073)
2θ range / º	4.508 to 54.148	5.024 to 49.526
Index ranges	-12 ≤ h ≤ 11, -18 ≤ k ≤ 18, -22 ≤ l ≤ 22	-14 ≤ h ≤ 14, -20 ≤ k ≤ 18, -30 ≤ l ≤ 32
Reflections collected	50409	65845
Independent reflections	9831 [R_{int} = 0.0738, R_{sigma} = 0.0622]	9932 [R_{int} = 0.0755, R_{sigma} = 0.0512]
Data/restraints/parameters	9831/0/507	9932/0/709
Goodness-of-fit on F^2	1.045	1.091
Final R indexes [$I > 2\sigma(I)$]	R_1 = 0.0788, wR_2 = 0.1670	R_1 = 0.0820, wR_2 = 0.2110
Final R indexes [all data]	R_1 = 0.1055, wR_2 = 0.1803	R_1 = 0.1044, wR_2 = 0.2316
Largest diff. peak/hole / (e Å^{-3})	0.55/-0.49	0.94/-0.69
CCDC number	2487856	2487857

UV-VIS ABSORPTION SPECTRA

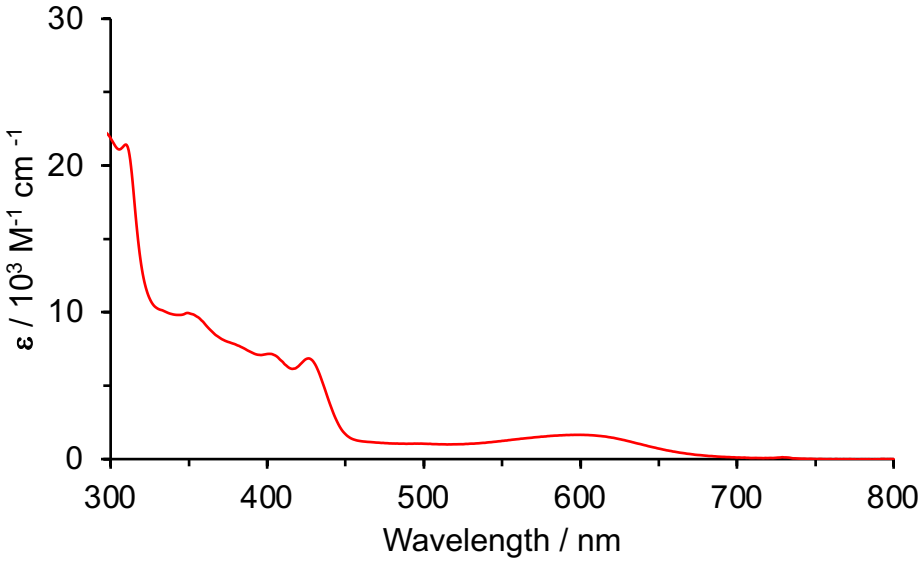

Figure S2. UV-vis absorption spectrum of **1** in acetonitrile.

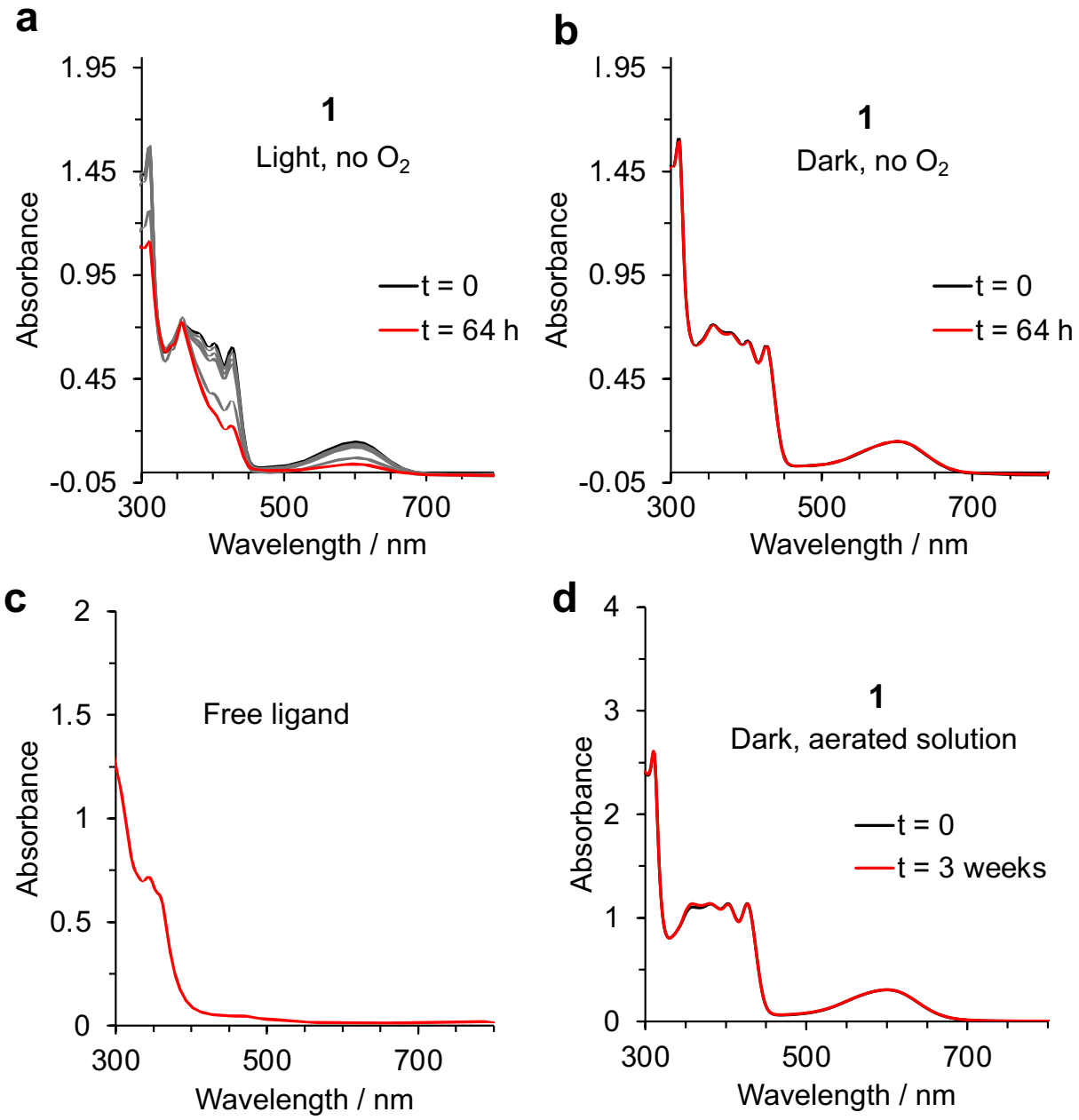

Figure S3. UV-vis absorption spectrum of (a) **1** monitored over 64 h under constant white-light irradiation in an N_2 atmosphere. The gray traces correspond to spectra collected between 0 and 64 hours. (b) **1** monitored over 64 h when stored in the dark in an N_2 atmosphere. (c) Proligand **L^L**. (d) **1** monitored over 3 weeks when stored in the dark as a solution in aerated acetonitrile.

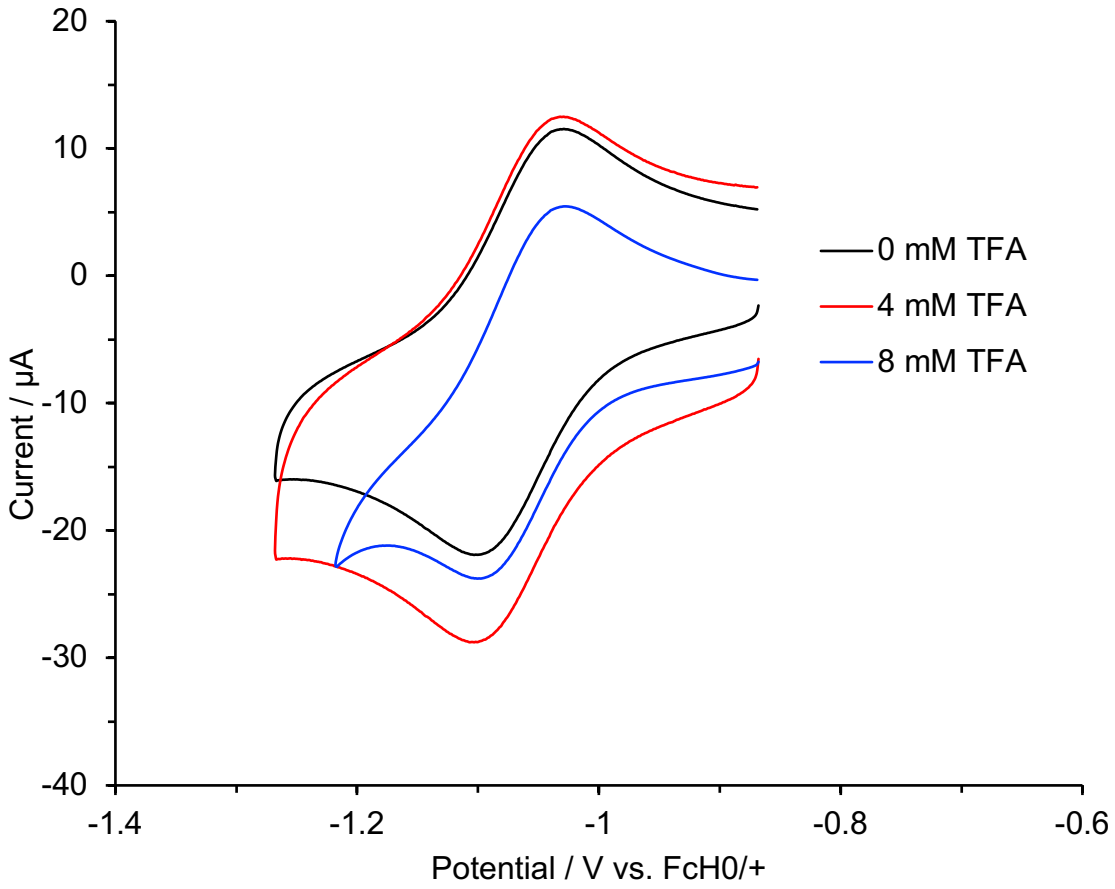

Figure S4. The first reduction event of **1** in the absence and presence of trifluoroacetic acid (0, 4 and 8 mM, respectively) showing that this event remains reversible in the presence of excess acid.

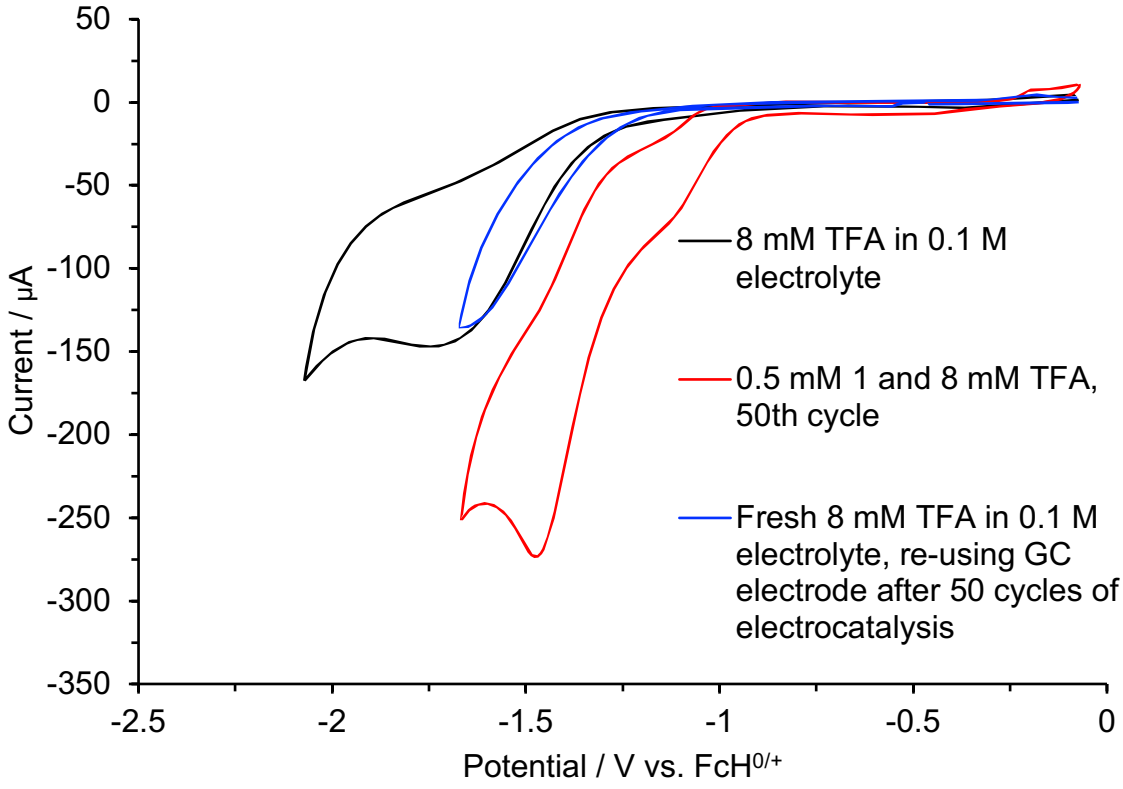

Figure S5. Control experiments to show that there is no electrodeposition on the working electrode following electrocatalysis. The black trace represents a CV trace of 8 mM TFA in 0.1 M nBu$_4$PF$_6$ (i.e., the 'blank') showing the reduction of TFA at -1.7 V on glassy carbon electrode. The red trace shows the 50th cycle by CV of 1 mM **1** and 8 mM TFA indicating constant electrocatalysis. The blue trace represents a CV of a fresh solution of 8 mM TFA in 0.1 M nBu$_4$PF$_6$ using the same GC electrode replaced to this new solution following the CV cycling represented by the red trace. The blue trace shows the same current response as the initial blank, indicating no electrocatalysis.

Calculation of Overpotential (η) for HER Catalysis

The overpotential was calculated by taking the half-wave potential of the catalytic wave (i.e. the potential at which half of the maximum current is observed) as the potential that needs to be applied for catalytic HER to occur in this system, and subtracting from it the standard potential for the reduction of protons from trifluoroacetic acid in acetonitrile:

$$\eta = E_{p/2} - E^0_{HA/H_2}$$

There are multiple ways to calculate/estimate E^0_{HA/H_2}. In our case, we calculated E^0_{HA/H_2} by taking into account the thermodynamic potential for H_2 evolution and the pK_a of TFA in acetonitrile, using the following equation derived by Evans:[4]

$$E^0_{HA/H_2} = E^0_{H^+/H_2} - \left(\frac{2.303\ RT}{F}\right) pK_{a,HA}$$

Using -0.028 V vs. Fc/Fc^+ as the standard potential for the solvated proton/dihydrogen couple reported using open circuit potentials in acetonitrile,[5] and 12.7 as the pK_a of trifluoroacetic acid in acetonitrile,[6] E^0_{HA/H_2} was calculated to be -0.779 V vs. Fc/Fc^+. Using -1.37 V vs. Fc/Fc^+ as the $E_{p/2}$ value for **1**, the overpotential could thus be calculated to be 591 mV.

COMPUTATIONAL DETAILS

All geometry optimizations were carried out using Gaussian 16 Rev. B01.[7] First, the geometry optimization and frequencies calculation of 1 was carried out in the gas phase using the O3LYP hybrid functional and coordinates from the crystal structure as the starting input, where three different basis sets (6-311G, LANL2TZ(f), and SDD) were tested. The obtained bond distances and bond angles around the coordination sphere of the metal were compared with the parameters from the crystal structure of the molecule. Even though all three optimized geometries were in agreement with the crystal structure, with an average deviation of less than 2% for each, it was found that LANL2TZ(f) gave the smallest average percent error from the crystal structure parameters. The geometry was then optimized in acetonitrile solvent using the SMD solvation model, where again the same three functionals were tested. Again, all three basis sets gave optimized geometries well within agreement of the crystal structure, with the average deviation from the crystal structure being less than 2%, but LANL2TZ(f) gave the smallest deviation.

The optimized coordinates obtained from O3LYP/LANL2TZ(f) in acetonitrile (SMD) were then used as the input for TD-DFT calculations. For all geometry optimizations, the absence of imaginary vibrational frequencies was used to confirm that the geometries were at a minimum on the potential energy surface. TD-DFT calculations were performed using Orca v.4.2.1[8–10] at the M06L/ZORA-def2-TZVP level of theory using the resolution of identity approximation (RIJCOSX)[11] and SARC/J auxiliary basis set, in acetonitrile, using the CPCM solvation model. These calculations were used to simulate the absorption spectrum of 1 in acetonitrile. The simulated spectrum was then generated using Multiwfn version 3.7[12] using a 0.37 eV broadening. The electron-hole density maps for the vertical excitations calculated during TD-DFT were

generated using the keepdens keyword and visualized using Multiwfn version 3.7,[12] at an isosurface value of 0.002, after generating molden files using the orca_2mkl module.

Table S3. Comparison of experimental and calculated bond distances and angles obtained using O3LYP functional and different basis sets (geometry optimization done in the gas phase).

Bond Length (Å)				
Bond	**Xtal structure**	**O3LYP/6-311G**	**O3LYP/LANL2TZ(f)**	**O3LYP/SDD**
Fe-N1	1.94459	1.97235	1.97286	1.98166
Fe-N2	1.95819	1.9723	1.97286	1.98169
Fe-N3	1.92184	1.90052	1.90738	1.91604
Fe-N4	1.91262	1.90053	1.90739	1.91609
Fe-P1	2.24181	2.31829	2.32196	2.32942
Fe-P2	2.23759	2.31822	2.32191	2.32942
Bond Angle (°)				
Bond	**Xtal structure**	**O3LYP/6-311G**	**O3LYP/LANL2TZ(f)**	**O3LYP/SDD**
N1-Fe-N4	90.5810	91.1358	91.1823	91.0743
N1-Fe-P1	85.8425	84.9151	84.9778	84.7833
N1-Fe-N2	80.2709	80.4367	80.5808	80.4336
N1-Fe-P2	164.6986	164.3471	164.5579	164.2716
N1-Fe-N3	88.1429	86.3014	86.4400	86.4149
N2-Fe-N4	88.1215	86.2984	86.4393	86.4110
N2-Fe-P1	165.4527	164.3428	164.5569	164.2705
N2-Fe-P2	85.1828	84.9171	84.9776	84.7823
N2-Fe-N3	91.9298	91.1409	91.1846	91.0770
N3-Fe-N4	176.6660	176.6479	176.8864	176.7137
N3-Fe-P1	91.4370	93.4147	93.3622	93.3445
N3-Fe-P2	89.6468	88.5095	88.4305	88.5363
N4-Fe-P1	87.7040	88.5046	88.4270	88.5334
N4-Fe-P2	93.6791	93.4125	93.3607	93.3400
P1-Fe-P2	108.9893	110.1524	109.8778	110.3980

Table S4. Comparison of experimental and calculated bond distances and angles obtained using O3LYP functional and different basis sets (geometry optimization done in acetonitrile).

Bond Length (Å)				
Bond	**Xtal structure**	**O3LYP/6-311G**	**O3LYP/LANL2TZ(f)**	**O3LYP/SDD**
Fe-N1	1.94459	1.9671	1.96782	1.97658
Fe-N2	1.95819	1.96709	1.96787	1.97674
Fe-N3	1.92184	1.9032	1.90946	1.91778
Fe-N4	1.91262	1.90315	1.9095	1.91781
Fe-P1	2.24181	2.31177	2.31596	2.32421
Fe-P2	2.23759	2.31174	2.31609	2.32441
Bond Angle (°)				
Bond	**Xtal structure**	**O3LYP/6-311G**	**O3LYP/LANL2TZ(f)**	**O3LYP/SDD**
N1-Fe-N4	90.5810	90.3742	90.4164	90.3834
N1-Fe-P1	85.8425	85.0242	85.0839	84.8645
N1-Fe-N2	80.2709	80.4341	80.5705	80.4266
N1-Fe-P2	164.6986	164.7086	164.9077	164.5631
N1-Fe-N3	88.1429	86.5345	86.6595	86.5787
N2-Fe-N4	88.1215	86.5324	86.6562	86.5780
N2-Fe-P1	165.4527	164.7051	164.9120	164.5684
N2-Fe-P2	85.1828	85.0259	85.0804	84.8609
N2-Fe-N3	91.9298	90.3735	90.4245	90.3982
N3-Fe-N4	176.6660	175.9518	176.1717	176.0329
N3-Fe-P1	91.4370	93.4708	93.3976	93.3732
N3-Fe-P2	89.6468	88.8633	88.8045	88.8875
N4-Fe-P1	87.7040	88.8595	88.8086	88.8906
N4-Fe-P2	93.6791	93.4636	93.4075	93.3940
P1-Fe-P2	108.9893	109.8260	109.5683	110.1487

Table S5. Average percent error between experimental and calculated bond distances and angles.

Gas Phase Geometry Optimizations			
	O3LYP/6-311G	**O3LYP/LANL2TZ(f)**	**O3LYP/SDD**
Average error in bond distances (%)	1.82	1.76	1.93
Average error in bond angles (%)	0.921	0.876	0.947
Geometry Optimizations in Acetonitrile (SMD Model)			
Average error in bond distances (%)	1.59	1.55	1.77
Average error in bond angles (%)	0.878	0.829	0.919

NMR SPECTRA

BKS-04-163-c4h.10.fid
second recrystalliation
PROTON CDCl3 {D:\nmrdata\user\Herbert} Herbert 21

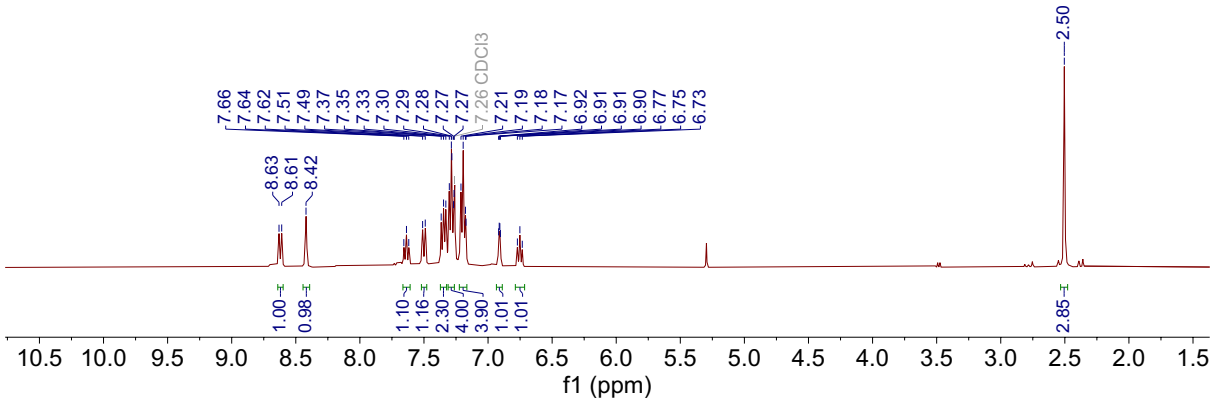

Figure S6. ^{1}H NMR spectrum ($CDCl_3$, 400 MHz, 22 °C) for **L^L**.

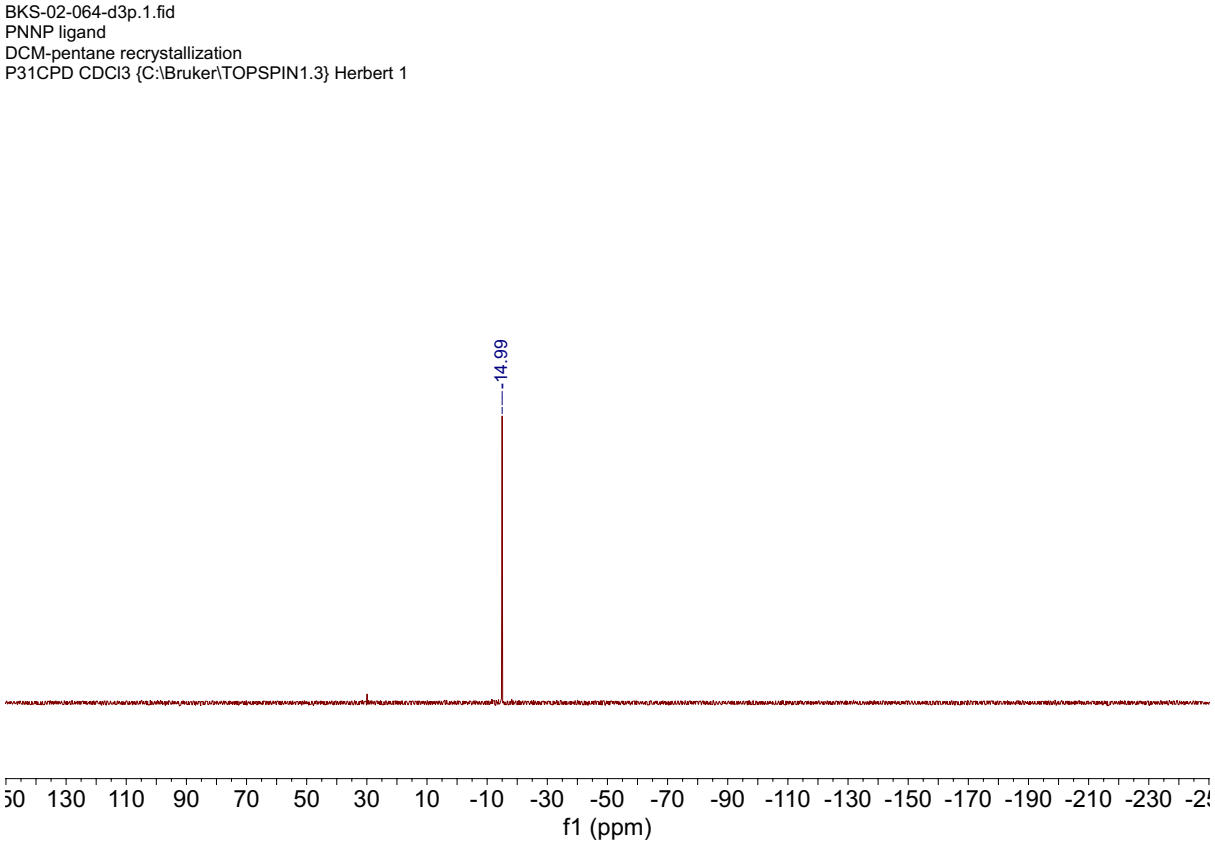

Figure S7. $^{31}P\{^{1}H\}$ NMR spectrum ($CDCl_3$, 121 MHz, 22 °C) for **L^L**.

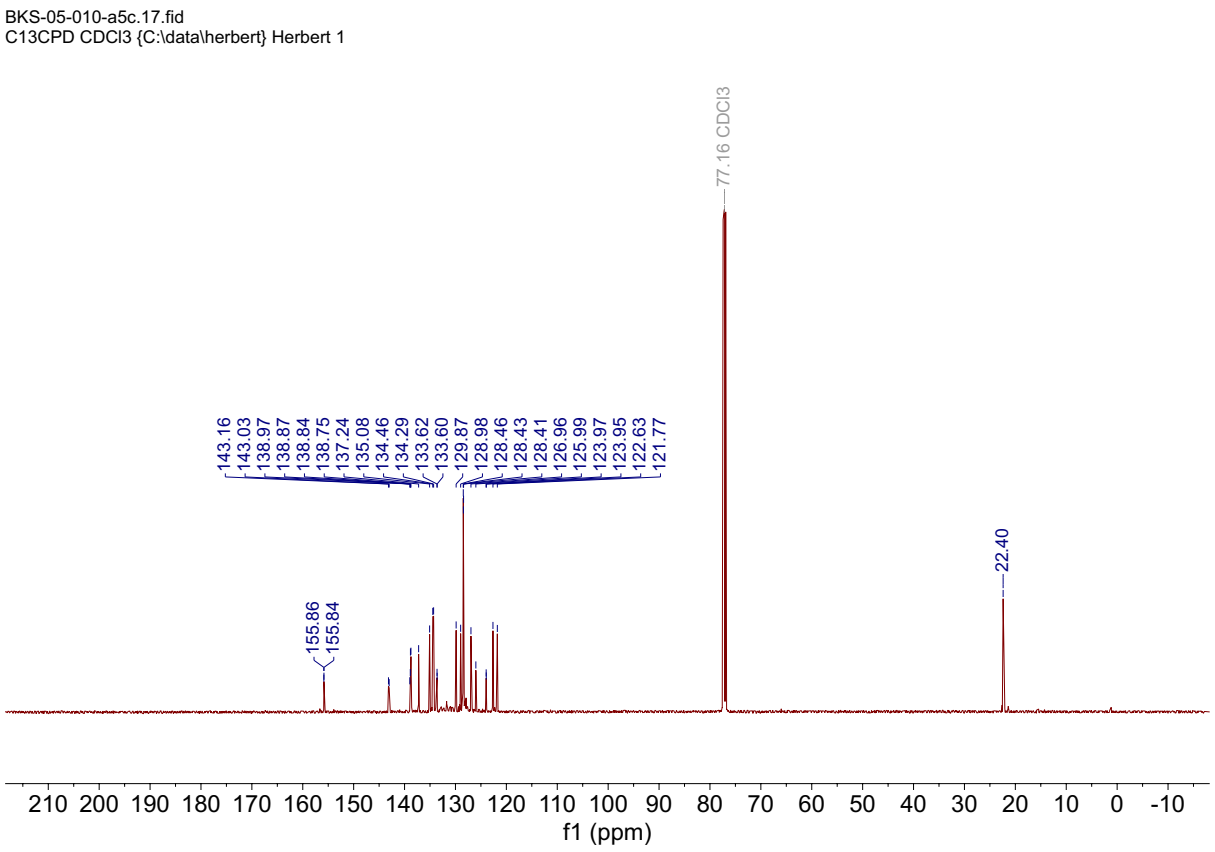

Figure S8. $^{13}C\{^{1}H\}$ NMR spectrum ($CDCl_3$, 126 MHz, 22 °C) for **L^L**.

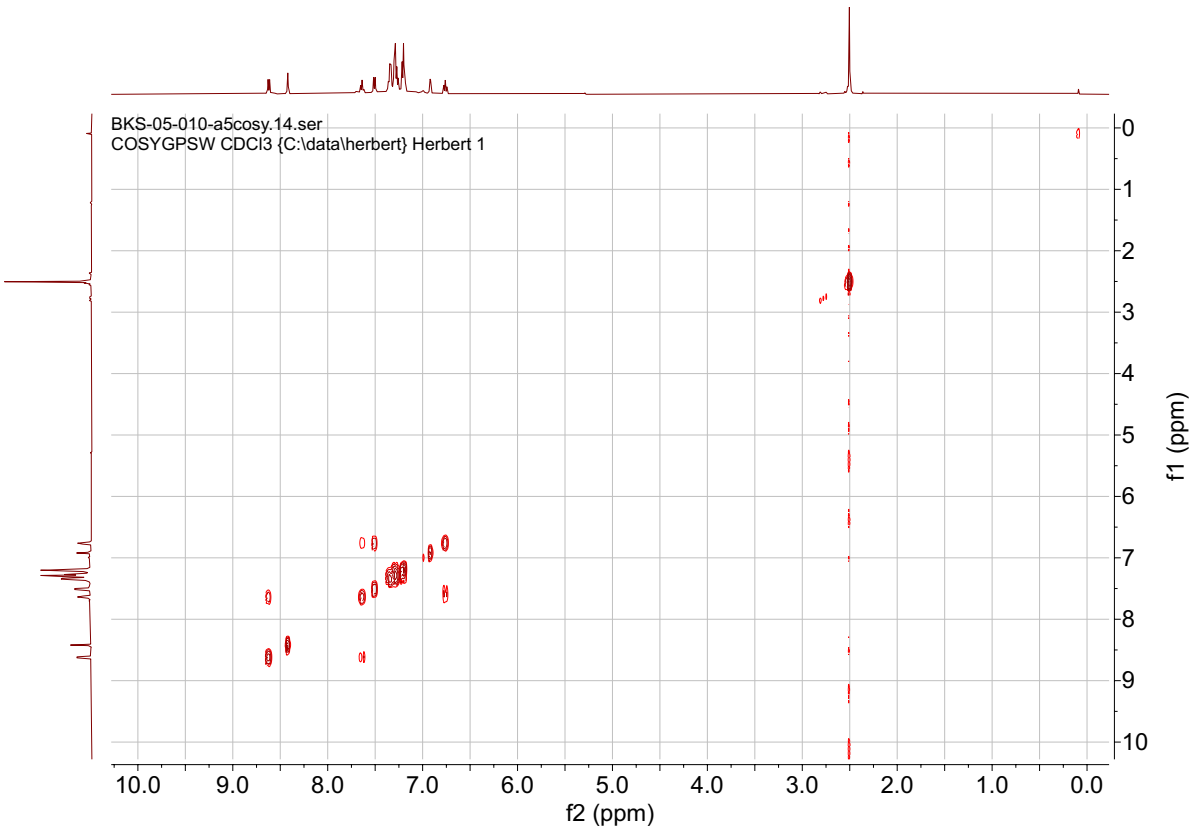

Figure S9. ^{1}H-^{1}H COSY NMR spectrum ($CDCl_3$, 500 MHz, 22 °C) of **L^L**.

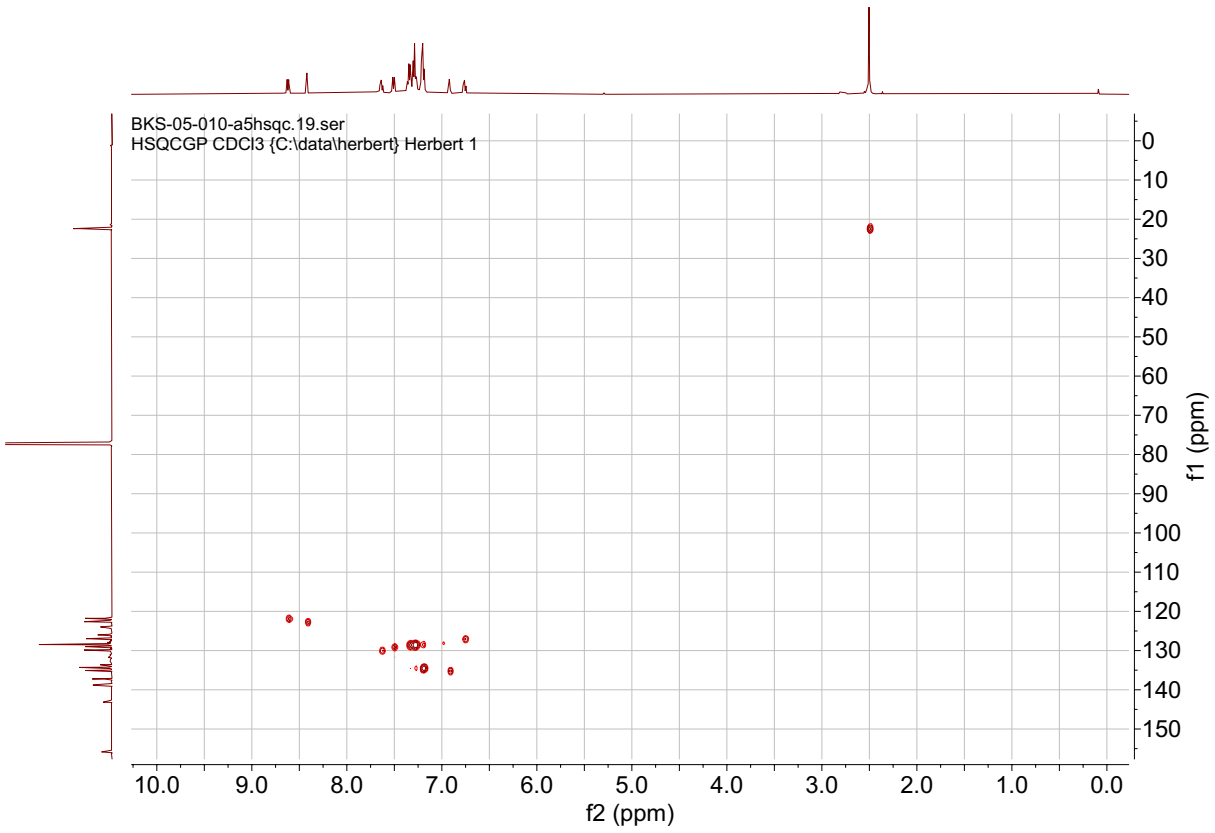

Figure S10. ^{1}H-^{13}C HSQC NMR spectrum ($CDCl_3$, 500/125 MHz, 22 °C) of **L^L**.

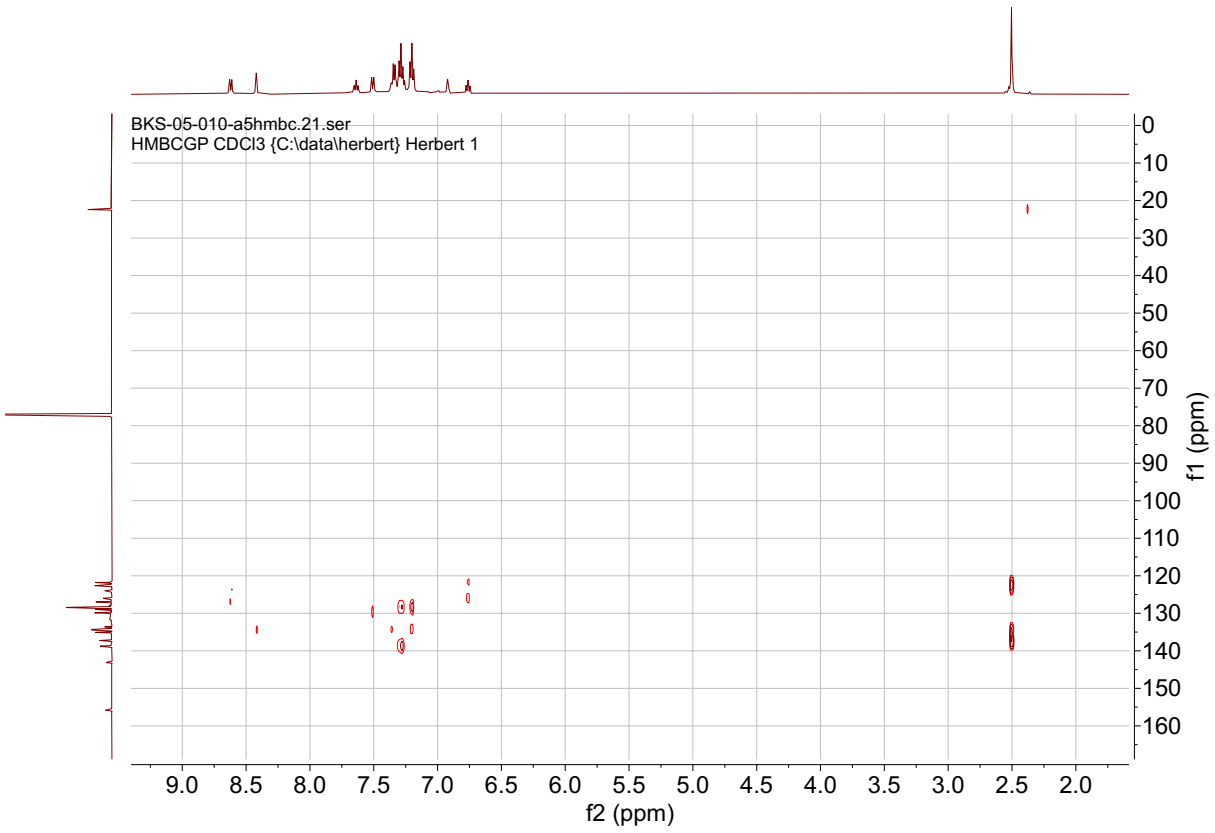

Figure S11. ^{1}H-^{13}C HMBC NMR spectrum ($CDCl_3$, 500/125 MHz, 22 °C) of **L^L**.

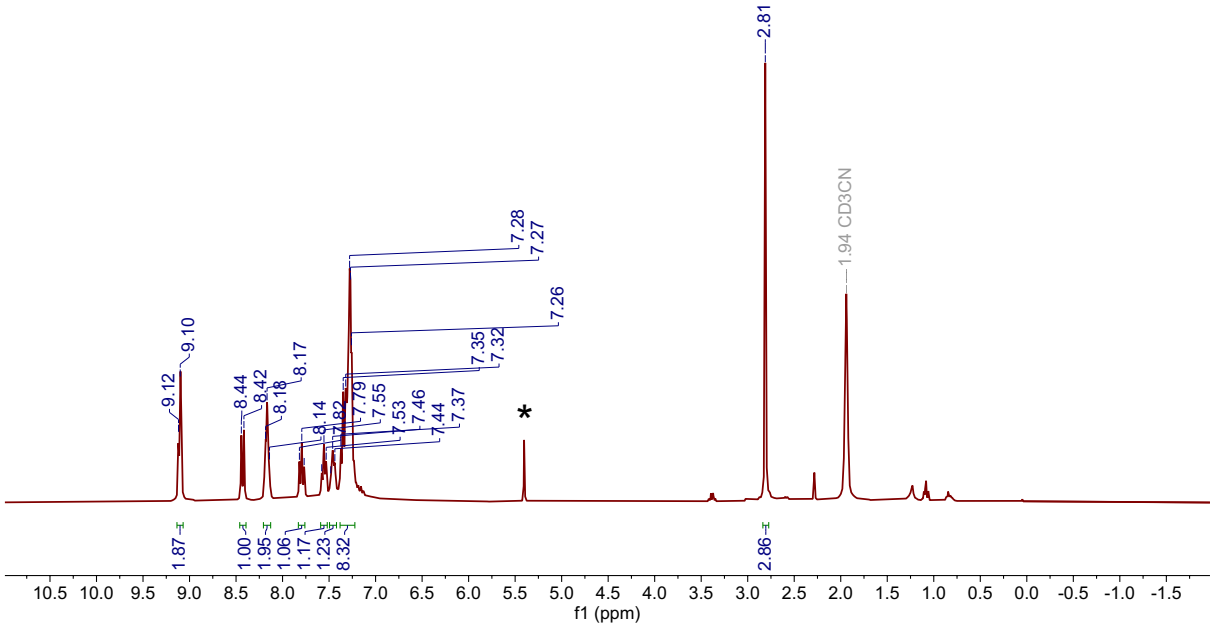

Figure S12. ^{1}H NMR spectrum (CD_3CN, 300 MHz, 22 °C) for **1**. Asterisk indicates residual solvent (dichloromethane).

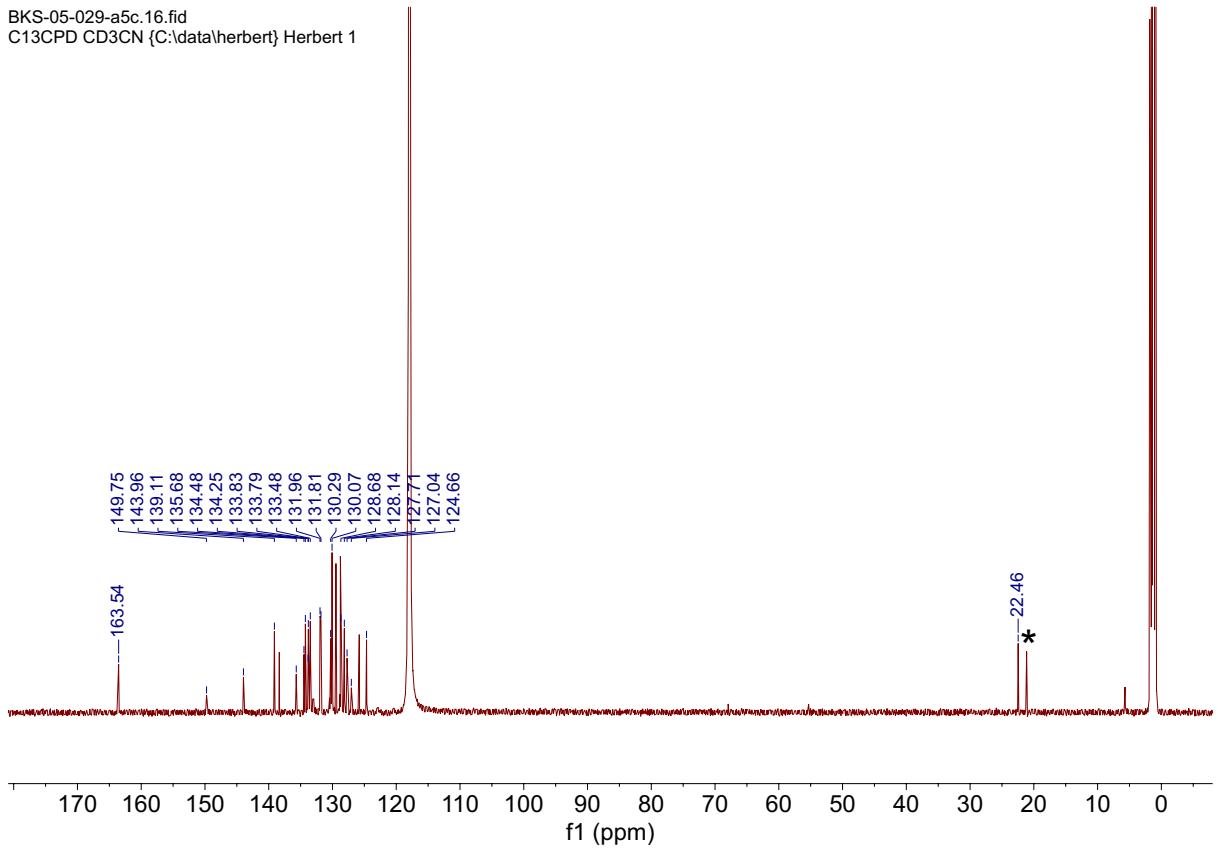

Figure S13. $^{13}C\{^{1}H\}$ NMR spectrum (CD_3CN, 126 MHz, 22 °C) for **1**. Asterisk indicates residual solvent (toluene).

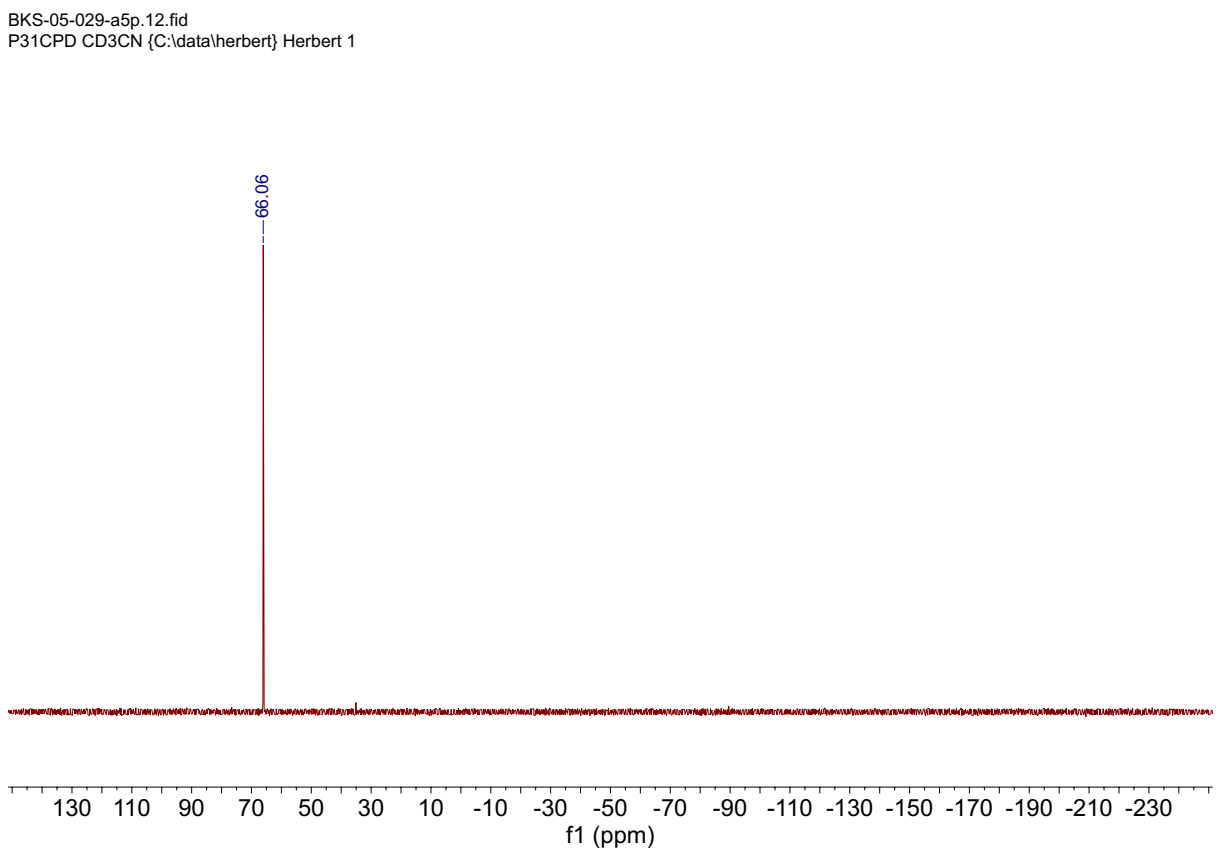

Figure S14. $^{31}P\{^{1}H\}$ NMR spectrum (CD_3CN, 202 MHz, 22 °C) for **1**.

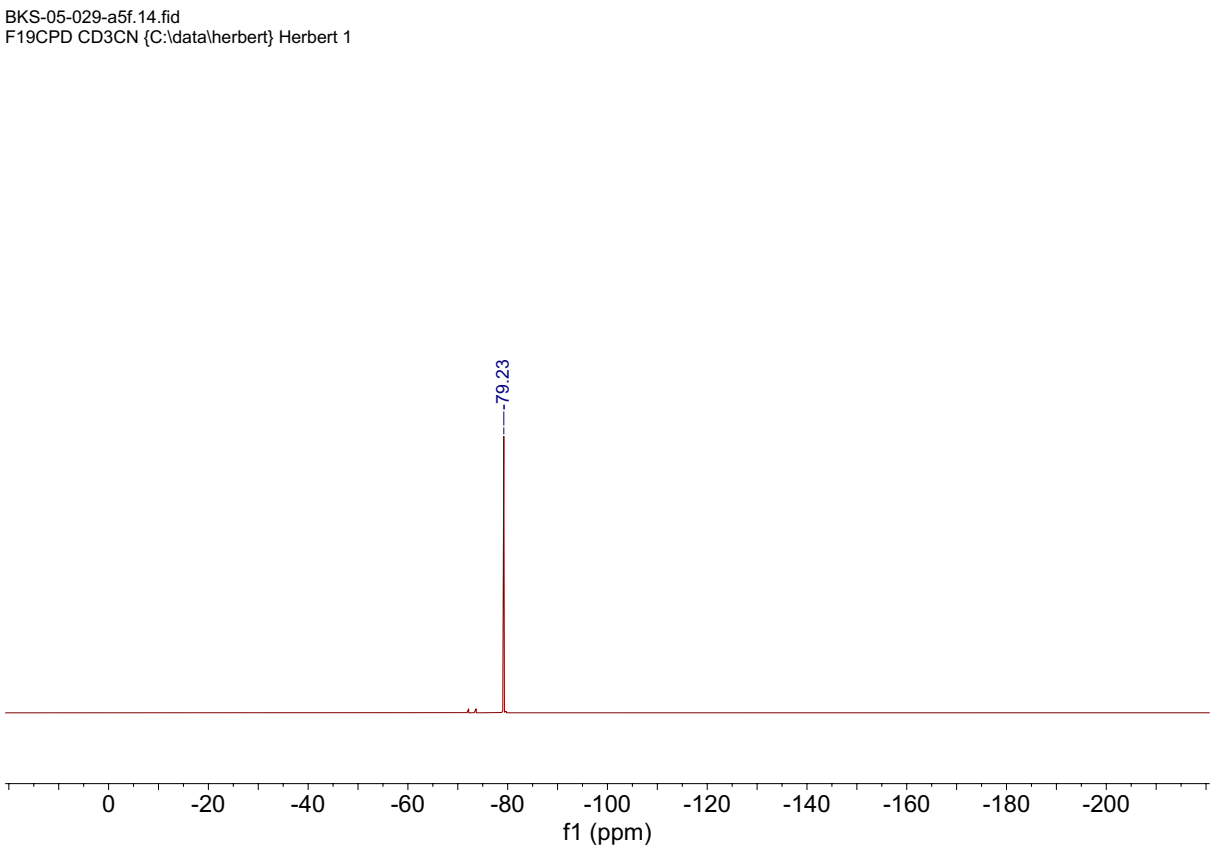

Figure S15. $^{19}F\{^{1}H\}$ NMR spectrum (CD_3CN, 471 MHz, 22 °C) for **1**.

HIGH RESOLUTION MASS SPECTRA

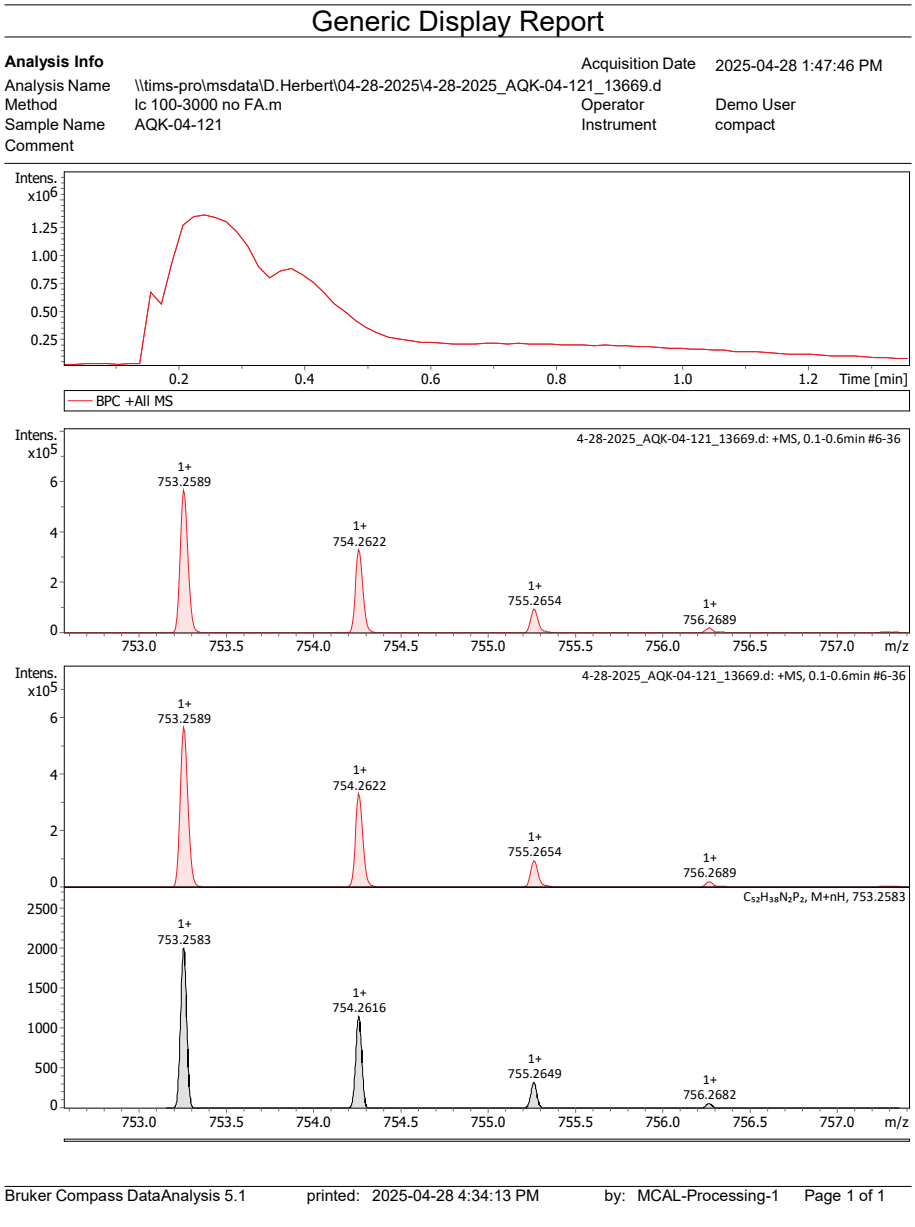

Figure S16. HR-MS of **L^L** showing the $(M+H)^+$ ion.

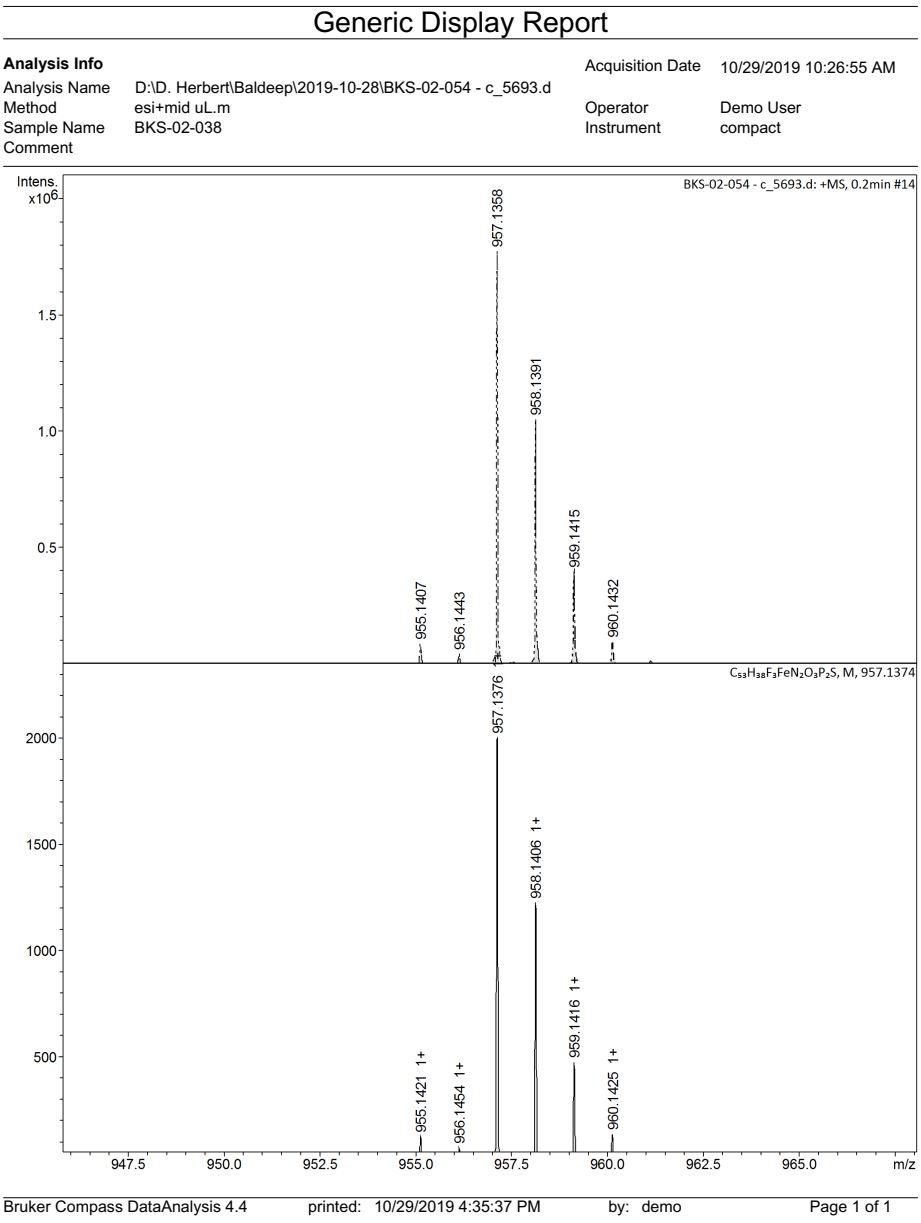

Figure S17. HR-MS of **1** showing the M^+ ion of M = $(C_{52}H_{38}FeN_2P_2)(CF_3SO_3)$ which corresponds to the loss of the two acetonitrile units and one triflate counterion during ionization.

References

(1) Mandapati, P.; Giesbrecht, P. K.; Davis, R. L.; Herbert, D. E. Phenanthridine-Containing Pincer-like Amido Complexes of Nickel, Palladium, and Platinum. *Inorg. Chem.* **2017**, *56*, 3674–3685.

(2) Mondal, R.; Lozada, I. B.; Davis, R. L.; Williams, J. A. G.; Herbert, D. E. Site-Selective Benzannulation of N-Heterocycles in Bidentate Ligands Leads to Blue-Shifted Emission from [(P^N)Cu]2(μ-X)2 Dimers. *Inorg. Chem.* **2018**, *57*, 4966–4978.

(3) Fulmer, G. R.; Miller, A. J. M.; Sherden, N. H.; Gottlieb, H. E.; Nudelman, A.; Stoltz, B. M.; Bercaw, J. E.; Goldberg, K. I. NMR Chemical Shifts of Trace Impurities: Common Laboratory Solvents, Organics, and Gases in Deuterated Solvents Relevant to the Organometallic Chemist. *Organometallics* **2010**, *29*, 2176–2179.

(4) Felton, G. A. N.; Glass, R. S.; Lichtenberger, D. L.; Evans, D. H. Iron-Only Hydrogenase Mimics. Thermodynamic Aspects of the Use of Electrochemistry to Evaluate Catalytic Efficiency for Hydrogen Generation. *Inorg. Chem.* **2006**, *45*, 9181–9184.

(5) Roberts, J. A. S.; Bullock, R. M. Direct Determination of Equilibrium Potentials for Hydrogen Oxidation/Production by Open Circuit Potential Measurements in Acetonitrile. *Inorg. Chem.* **2013**, *52*, 3823–3835.

(6) Fourmond, V.; Jacques, P.-A.; Fontecave, M.; Artero, V. H2 Evolution and Molecular Electrocatalysts: Determination of Overpotentials and Effect of Homoconjugation. *Inorg. Chem.* **2010**, *49*, 10338–10347.

(7) Frisch, M. J.; Trucks, G. W.; Schlegel, H. B.; Scuseria, G. E.; Robb, M. A.; Cheeseman, J. R.; Scalmani, G.; Barone, V.; Petersson, G. A.; Nakatsuji, H.; Li, X.; Caricato, M.; Marenich, A. V.; Bloino, J.; Janesko, B. G.; Gomperts, R.; Mennucci, B.; Hratchian, H. P.; Ortiz, J. V.; Izmaylov, A. F.; Sonnenberg, J. L.; Williams; Ding, F.; Lipparini, F.; Egidi, F.; Goings, J.; Peng, B.; Petrone, A.; Henderson, T.; Ranasinghe, D.; Zakrzewski, V. G.; Gao, J.; Rega, N.; Zheng, G.; Liang, W.; Hada, M.; Ehara, M.; Toyota, K.; Fukuda, R.; Hasegawa, J.; Ishida, M.; Nakajima, T.; Honda, Y.; Kitao, O.; Nakai, H.; Vreven, T.; Throssell, K.; Montgomery Jr., J. A.; Peralta, J. E.; Ogliaro, F.; Bearpark, M. J.; Heyd, J. J.; Brothers, E. N.; Kudin, K. N.; Staroverov, V. N.; Keith, T. A.; Kobayashi, R.; Normand, J.; Raghavachari, K.; Rendell, A. P.; Burant, J. C.; Iyengar, S. S.; Tomasi, J.; Cossi, M.; Millam, J. M.; Klene, M.; Adamo, C.; Cammi, R.; Ochterski, J. W.; Martin, R. L.; Morokuma, K.; Farkas, O.; Foresman, J. B.; Fox, D. J. Gaussian 16 Rev. B.01, 2016.

(8) Neese, F. The ORCA Program System. *WIREs Comp. Mol. Sci.* **2012**, *2*, 73–78.

(9) Neese, F.; Wennmohs, F.; Becker, U.; Riplinger, C. The ORCA Quantum Chemistry Program Package. *J. Chem. Phys.* **2020**, *152*, 224108.

(10) Neese, F. Software Update: The ORCA Program System, Version 4.0. *WIREs Comp. Mol. Sci.* **2018**, *8*, e1327.

(11) Neese, F.; Wennmohs, F.; Hansen, A.; Becker, U. Efficient, Approximate and Parallel Hartree–Fock and Hybrid DFT Calculations. A 'Chain-of-Spheres' Algorithm for the Hartree–Fock Exchange. *Chem. Phys.* **2009**, *356*, 98–109.

(12) Lu, T.; Chen, F. Multiwfn: A Multifunctional Wavefunction Analyzer. *J. Comput. Chem.* **2012**, *33*, 580–592.